B7-H1 shapes T-cell–mediated brain endothelial cell dysfunction and regional encephalitogenicity in spontaneous CNS autoimmunity

Luisa Klotz[a,1], Ivan Kuzmanov[a,1], Stephanie Hucke[a], Catharina C. Gross[a], Vilmos Posevitz[a,2], Angela Dreykluft[b,3], Andreas Schulte-Mecklenbeck[a], Claudia Janoschka[a], Maren Lindner[a], Martin Herold[a], Nicholas Schwab[a], Isis Ludwig-Portugall[c], Christian Kurts[c], Sven G. Meuth[a], Tanja Kuhlmann[d], and Heinz Wiendl[a,4]

[a]Department of Neurology, University Hospital Münster, 48149 Muenster, Germany; [b]Department of Neurology, University Hospital Würzburg, 97080 Wuerzburg, Germany; [c]Institute of Experimental Immunology, University of Bonn, 53127 Bonn, Germany; and [d]Institute for Neuropathology, University of Münster, 48149 Muenster, Germany

Edited by Lawrence Steinman, Stanford University School of Medicine, Stanford, CA, and approved August 11, 2016 (received for review January 27, 2016)

Molecular mechanisms that determine lesion localization or phenotype variation in multiple sclerosis are mostly unidentified. Although transmigration of activated encephalitogenic T cells across the blood–brain barrier (BBB) is a crucial step in the disease pathogenesis of CNS autoimmunity, the consequences on brain endothelial barrier integrity upon interaction with such T cells and subsequent lesion formation and distribution are largely unknown. We made use of a transgenic spontaneous mouse model of CNS autoimmunity characterized by inflammatory demyelinating lesions confined to optic nerves and spinal cord (OSE mice). Genetic ablation of a single immune-regulatory molecule in this model [i.e., B7-homolog 1 (B7-H1, PD-L1)] not only significantly increased incidence of spontaneous CNS autoimmunity and aggravated disease course, especially in the later stages of disease, but also importantly resulted in encephalitogenic T-cell infiltration and lesion formation in normally unaffected brain regions, such as the cerebrum and cerebellum. Interestingly, B7-H1 ablation on myelin oligodendrocyte glycoprotein-specific CD4$^+$ T cells, but not on antigen-presenting cells, amplified T-cell effector functions, such as IFN-γ and granzyme B production. Therefore, these T cells were rendered more capable of eliciting cell contact-dependent brain endothelial cell dysfunction and increased barrier permeability in an in vitro model of the BBB. Our findings suggest that a single immune-regulatory molecule on T cells can be ultimately responsible for localized BBB breakdown, and thus substantial changes in lesion topography in the context of CNS autoimmunity.

neuroinflammation | multiple sclerosis | spontaneous EAE | CNS lesion distribution | blood–brain barrier

Multiple sclerosis (MS) is the most common chronic inflammatory demyelinating disease of the CNS. Disease pathogenesis is initiated by peripheral activation of autoimmune T lymphocytes by yet unknown mechanisms, followed by T-cell expansion and subsequent migration across the complex structure of the blood–brain barrier (BBB). Within the CNS, entry of this first wave of T cells elicits recruitment of other immune cells, which together evoke a local inflammatory process ultimately resulting in demyelination, as well as axonal and neuronal damage (1). Several histological MS subtypes have been described with regard to lesion distribution and cellular composition (2). The reasons underlying distinct lesion development at different anatomical sites still remain however largely elusive: Some authors have proposed that the nature and expression pattern of the target autoantigen might play a role (3, 4). Others have observed an influence of the HLA complex and its role in shaping antigen presentation, thus suggesting that T-cell antigen specificity might impact the location of inflammation (5). Additionally, T-cell polarization into distinct T helper subtypes, as well as their expression pattern of chemokine receptors and adhesion molecules, has been implicated in determining the localization of inflammatory lesions within the CNS (6–8).

With respect to the very onset of lesion development, imaging techniques have revealed that a local dysregulation of the BBB integrity already precedes lesion formation (9, 10). Moreover, in a recent study, Maggi et al. observed an association between early changes in BBB permeability and perivascular inflammatory cuffing (11). However, the mechanisms causing local BBB dysfunction as an initial step in MS lesion formation still remain to be resolved.

Animal models of CNS autoimmunity, especially the models of experimental autoimmune encephalomyelitis (EAE), have

Significance

A crucial step in the pathogenesis of autoimmune diseases, such as multiple sclerosis (MS), is transmigration of pathogenic T cells across the blood–brain barrier. These T cells mediate inflammation and subsequent lesion formation in the CNS. However, molecular mechanisms underlying lesion distribution and formation are not well understood. We here show that genetic ablation of a single immunoregulatory molecule on T cells, B7-homolog 1 (B7-H1), causes local endothelial dysfunction and determines lesion topography in a spontaneous mouse model of CNS autoimmunity. These findings can lead to new therapeutic approaches in targeting pathogenic T cell responses in MS.

Author contributions: L.K., I.K., S.H., C.C.G., V.P., A.D., A.S.-M., C.J., M.L., M.H., N.S., I.L.-P., C.K., S.G.M., T.K., and H.W. designed research; I.K., S.H., A.D., A.S.-M., C.J., M.H., and T.K. performed research; L.K., I.K., S.H., A.D., C.J., M.L., M.H., T.K., and H.W. analyzed data; and L.K., I.K., M.L., and H.W. wrote the paper.

Conflict of interest statement: L.K. received compensation for serving on Scientific Advisory Boards for Genzyme and Novartis; received speaker honoraria and travel support from Novartis, Merck Sorono, and CSL Behring; and receives research support from Novartis and Biogen Idec. C.C.G. received speaker honoraria and travel expenses for attending meetings from Genzyme (2014), Novartis Pharma GmbH (2011), and Bayer Health Care (2014). N.S. received speaking honoraria from Novartis and Biogen and travel expenses from Biogen. S.G.M. received honoraria for lecturing and travel expenses for attending meetings and financial research support from Bayer, Bayer Schering, Biogen Idec, Genzyme, Merck Serono, Novartis, Omniamed, Novo Nordisk, Sanofi-Aventis, and Teva. T.K. received honoraria for lectures from Novartis and Biogen Idec Canada and served as a consultant for Genzyme Corporation. H.W. received compensation for serving on Scientific Advisory Boards/Steering Committees for Bayer Healthcare, Biogen Idec, Genzyme, Merck Serono, Novartis, and Sanofi Aventis; received speaker honoraria and travel support from Bayer Vital GmbH, Bayer Schering AG, Biogen Idec, CSL Behring, Fresenius Medical Care, Genzyme, Glaxo Smith Kline, GW Pharmaceuticals, Lundbeck, Merck Serono, Omniamed, Novartis, and Sanofi Aventis; received compensation as a consultant from Biogen Idec, Merck Serono, Novartis, and Sanofi Aventis; and received research support from Bayer Vital, Biogen Idec, Genzyme, Merck Serono, Novartis, Sanofi Aventis Germany, and Sanofi US.

This article is a PNAS Direct Submission.

Freely available online through the PNAS open access option.

[1]L.K. and I.K. contributed equally to this work.

[2]Present address: Ganymed Pharmaceuticals AG, 55131 Mainz, Germany.

[3]Present address: SOMNOmedics GmbH, 97236 Randersacker, Germany.

[4]To whom correspondence should be addressed. Email: heinz.wiendl@ukmuenster.de.

This article contains supporting information online at www.pnas.org/lookup/suppl/doi:10.1073/pnas.1601350113/-/DCSupplemental.

been of great value in elucidating crucial steps in disease pathogenesis. Up to now, a broad range of different models with distinct features have been available, the most commonly used of them induced by immunization of susceptible rodents with myelin antigens or adoptive transfer of highly activated myelin-reactive T cells. However, these models are of limited value for studying the very first steps of disease initiation and lesion development, mainly due to their dependence on microbial adjuvants for artificial breakdown of tolerance and promotion of BBB disruption (12–14). During the last years, novel models of spontaneous CNS autoimmunity have been developed by crossing myelin-specific T-cell receptor (TCR) transgenic mice and myelin-specific Ig heavy chain knock-in mice (3, 15). The offspring of those mice are characterized by spontaneous development of a severe form of EAE. Lesions here are confined to the spinal cord and optic nerves, making this model an interesting tool for further investigation of the determinants of lesion development and lesion distribution under "homeostatic", non–vaccine-depending immune-regulatory conditions.

We investigated the hypothesis whether and how genetic modification of single immune-regulatory molecules could influence lesion distribution and phenotype variation in genetically susceptible hosts. We thus used the opticospinal EAE (OSE) model and genetically modulated an immune-regulatory molecule, B7-homolog 1 (B7-H1). Absence of B7-H1 increased incidence of spontaneous CNS autoimmunity and aggravated disease course. Importantly, B7-H1 ablation on T cells, but not on antigen-presenting cells (APCs), enhanced their capacity to elicit brain endothelial cell (EC) dysfunction in a cell contact-dependent fashion in an in vitro model of the BBB and increased BBB permeability both in vitro and in vivo. Our findings suggest that single immune regulatory molecules that alter the activation status of encephalitogenic T cells can influence lesion distribution, which is associated with an altered capacity of these cells to elicit transient focal EC dysfunction and barrier dysfunction as essential steps for lesion development.

Results

Ablation of B7-H1 Increases Disease Incidence and Severity in OSE Mice Associated with Altered Lesion Distribution. To assess the relevance of B7-H1 in the context of spontaneous CNS autoimmunity, we generated mice that both lack B7-H1 on all cells and harbor myelin oligodendrocyte glycoprotein (MOG)-specific T-cell receptor (TCR) transgenic T cells as well as MOG-specific Ig heavy-chain transgenic B cells on a C57BL/6 background ($B7\text{-}H1^{KO} \times TCR^{MOG} \times IgH^{MOG}$, for simplification named OSE^{KO}). As described in the literature, double transgenic $TCR^{MOG} \times IgH^{MOG}$ mice (here named OSE^{WT} mice) develop spontaneous inflammatory demyelinating lesions in the spinal cord and the optic nerve, with an average disease incidence of ∼50 to 70% (3). Strikingly, additional lack of B7-H1 in these mice resulted in a highly significant increase in disease incidence, resulting in a nearly 100% disease penetrance (93% in OSE^{KO} mice compared with 69% in OSE^{WT} mice) (Fig. 1*A*). Moreover, OSE^{KO} mice exhibited an aggravated disease course, especially in later disease stages, as reflected by a highly significant change in the median survival from 103 d in OSE^{WT} mice to 72 d in OSE^{KO} mice (Fig. 1*B*). These profound differences in disease severity have been observed in two independent cohorts of mice encompassing more than 215 mice per group (Fig. S1 and Table S1). However, early disease course was only slightly aggravated in OSE^{KO} mice (Fig. 1*C*). Interestingly, quantitative histological analysis of spinal cord infiltrates from score-matched 12 OSE^{WT} mice and 10 OSE^{KO} mice (mean score 5.75) did not reveal any alterations with regard to the size of the inflamed area and leptomeningeal infiltrates, as well as T-cell numbers in spinal cord leptomeninges and parenchyma (Fig. 1 *D* and *E*). In contrast to that finding, detailed histological analysis of other brain regions classically spared in this animal model (3) revealed a significant increase in T-cell infiltrates within the cerebellum and brainstem regions in OSE^{KO} mice compared with OSE^{WT} mice and the presence of T-cell infiltrates in the cerebrum of 8 out of 10 OSE^{KO} mice compared with 1 out of 12 OSE^{WT} mice (Fig. 1*E*, *Bottom*). Together, these data indicate that OSE^{KO} mice exhibit an enhanced disease severity at later stages, resulting in increased mortality combined with inflammatory lesion development in regions normally spared in this model.

A detailed analysis of these brain infiltrates in OSE^{KO} mice further revealed only a few T cells within the choroid plexus and leptomeninges and a clear predominance of T-cell infiltrates within the perivascular areas (Fig. 1*F*). These T-cell infiltrates did not contain $CD8^+$ T cells (Fig. S2*A*). Our histological findings were accompanied by significantly increased numbers of CNS infiltrating $CD4^+$ T cells in the cerebellum and brainstem of OSE^{KO} compared with OSE^{WT} mice. This finding was also determined by quantitative flow cytometry at the very early stage of disease (Fig. 2*B*) whereas $CD4^+$ T-cell numbers in spinal cord and optic nerves—the classical predilection sites of CNS inflammation in this model—were again not different between OSE^{KO} and OSE^{WT} mice at this time point (Fig. 2*B*). There was a trend toward increased $CD4^+$ T-cell numbers in the cerebrum of OSE^{KO} mice compared with OSE^{WT} mice; however, this trend did not reach statistical significance, probably due to the overall low number of isolated immune cells from this large brain area. Of note, frequencies of MOG-specific transgenic $CD4^+$ T cells were not different in OSE^{KO} mice compared with OSE^{WT} mice, and these transgenic T cells accounted for more than 90% of all $CD4^+$ T cells in both strains (Fig. 2*A*). Further flow cytometric analysis of cerebellum and brainstem areas, as well as spinal cords, revealed no differences in numbers of infiltrating $CD8^+$ T cells and $FoxP3^+$ regulatory T cells but a slight increase in B cells and myeloid cells in the cerebellum/brainstem of OSE^{KO} mice, without any differences in spinal cords (Fig. 2*C* and Fig. S2*C*). Together, these data suggest that altered lesion topography in OSE^{KO} mice is driven by MOG-specific $CD4^+$ T cells, with a concomitant rise in other non–T-cell subpopulations, such as B cells and myeloid cells.

Ablation of B7-H1 on T Cells Augments T-Cell Effector Functions. Based on our findings so far, we next characterized MOG-specific $CD4^+$ T-cell responses in the periphery of OSE^{KO} compared with OSE^{WT} mice with established disease (score-matched mice with a mean score of 4). Also, in these score-matched mice, the frequency of MOG-specific transgenic T cells within the $CD4^+$ T-cell population was not altered (Fig. 3*A*). However, diseased OSE^{KO} mice exhibited significantly increased lymph node cell numbers, as well as absolute numbers of MOG-specific $CD4^+$ T cells within lymph nodes, compared with OSE^{WT} mice (Fig. 3*A*), suggesting a pronounced expansion of autoreactive T cells in the peripheral immune compartment of OSE mice lacking the immune-inhibitory molecule B7-H1. Along these lines, absolute numbers of cytokine and granzyme B-producing MOG-specific $CD4^+$ T cells were significantly increased in the lymph nodes of OSE^{KO} compared with OSE^{WT} mice (Fig. 3*B*), which was observed for a broad range of effector molecules (including IFN-γ, granzyme B, TNF-α, GM-CSF, IL-2, and IL-17A), indicating that there is no shift in T helper-cell polarization in OSE^{KO} mice (Fig. 3*B*). Percentages of effector molecule-producing MOG-specific T cells within the $CD4^+$ T-cell population, as well as effector molecule production on a per cell basis assessed by mean fluorescence intensity (MFI), were not altered in OSE^{KO} mice (Fig. S3 *B* and *C*).

Along these lines, we also observed an increase in absolute numbers of MOG-specific $CD4^+$ T cells in brains of score-matched OSE^{KO} compared with OSE^{WT} mice (Fig. 3*C*) and, accordingly, an increase in absolute numbers of MOG-specific T cells expressing IFN-γ and granzyme B (Fig. 3*C*) whereas percentages of transgenic T cells producing these effector molecules were again unchanged (Fig. S3 *D* and *E*). Together, these data indicate that OSE^{KO} mice exhibit enhanced quantitative but

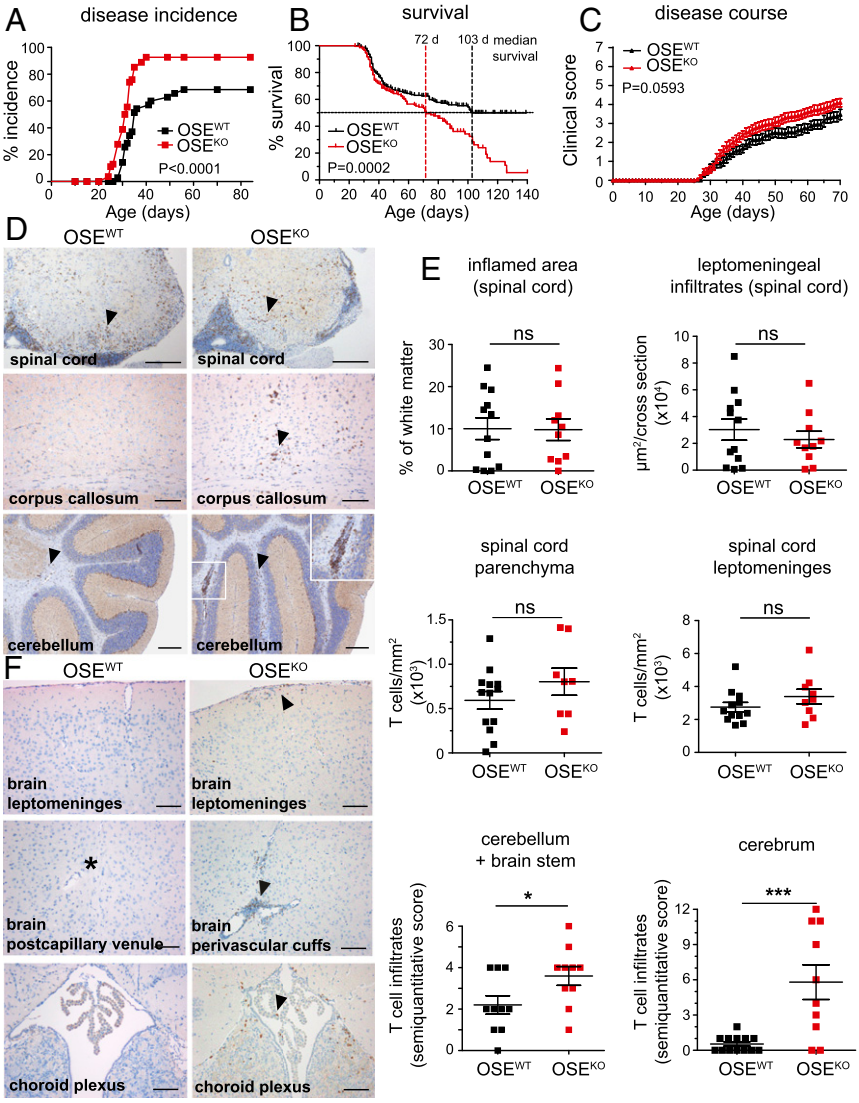

Fig. 1. B7-H1 restricts spontaneous CNS autoimmunity and prevents T-cell infiltration into the brain of sick OSE mice. (*A*) Percentages of OSE^{WT} and OSE^{KO} mice that spontaneously developed EAE symptoms over a period of 12 wk after birth. Forty-five OSE^{WT} and 57 OSE^{KO} mice were analyzed. (*B*) Survival of 246 OSE^{WT} and 216 OSE^{KO} mice was monitored over a period of 140 d after birth. Mice were recorded as dead when they reached the clinical score 5.5 or higher; mice eliminated for reasons unrelated to disease course (all with score below 5.5) were censored (indicated by vertical ticks). (*C*) Clinical scores of 18 OSE^{WT} and 18 OSE^{KO} mice until 70 d of age. (*D–F*) Immunohistochemical analysis of T-cell infiltration in different CNS regions of 12 OSE^{WT} and 10 OSE^{KO} mice (score-matched, mean clinical score 5.75). (*D*) Representative images of T-cell infiltrates in the spinal cord, corpus callosum, and cerebellum, as indicated. (*E*) Quantification of the extent of inflammation and T-cell infiltration in the spinal cord parenchyma and leptomeninges, as indicated (*Top* and *Middle*); semiquantitative scores of T-cell infiltration in the cerebellum and brainstem, and in the cerebrum (*Bottom*). (*F*) Representative images of T-cell infiltration in different brain areas of OSE^{WT} and OSE^{KO} mice. (*D* and *F*) T cells are indicated by arrowheads. The asterisk in *F* indicates a postcapillary venule. (Scale bars: *D*, spinal cord, 200 µm; corpus callosum, 100 µm; cerebellum, 200 µm; *F*, 100 µm.) (*E*) Each data point represents one mouse. (*A* and *B*) Log-rank (Mantel–Cox) test. (*C*) Two-way ANOVA with Bonferroni correction for multiple comparisons. (*E*) Unpaired, two-tailed Student's *t* test. *$P < 0.05$; ***$P < 0.001$; ns, not significant.

not qualitative MOG-specific CD4$^+$ effector T-cell responses both in the periphery and in the brain. These differences were not caused by differences in disease severity because score-matched mice were used for analysis.

We next went on to evaluate how lack of B7-H1 might affect initial T-cell activation as a first putative step in disease pathogenesis. Based on the well-known role of B7-H1 on APCs in control of T-cell activation and T-cell–mediated autoimmunity (16–18), we performed coculture assays using MOG-specific B cells from Th mice as APCs and MOG-specific CD4$^+$ T cells from 2D2 mice. Surprisingly, lack of B7-H1 on antigen-presenting B cells did not result in enhanced T-cell activation as evaluated by quantification of IFN-γ production (Fig. 4*A*) and T-cell expansion (Fig. 4*B*). In sharp contrast, lack of B7-H1 on T cells resulted in significantly enhanced T-cell responses reflected by increased IFN-γ production as well as augmented T-cell expansion (Fig. 4 *C* and *D* and Fig. S4*B*). Of note, WT T cells also displayed an enhanced IFN-γ production in the presence of a neutralizing antibody against B7-H1 (Fig. 4*E*). Evaluation of other key proinflammatory cytokines revealed that increased cytokine production by B7-H1^{KO} T cells was basically confined to IFN-γ because levels of IL-2, TNF-α, GM-CSF, and IL-17A remained unchanged, thus indicating that also in vitro there was no shift in T helper-cell polarization in the absence of B7-H1 (Fig. 4*F* and Fig. S4*D*). Moreover, detailed analysis of a broad range of T-cell activation markers, as well as costimulatory molecules, did not reveal any differences between naïve, as well as activated, B7-H1^{KO} T cells compared with WT T cells (Fig. 4 *G* and *H* and Fig. S4*D*). Along these lines, the activation status of B cells upon

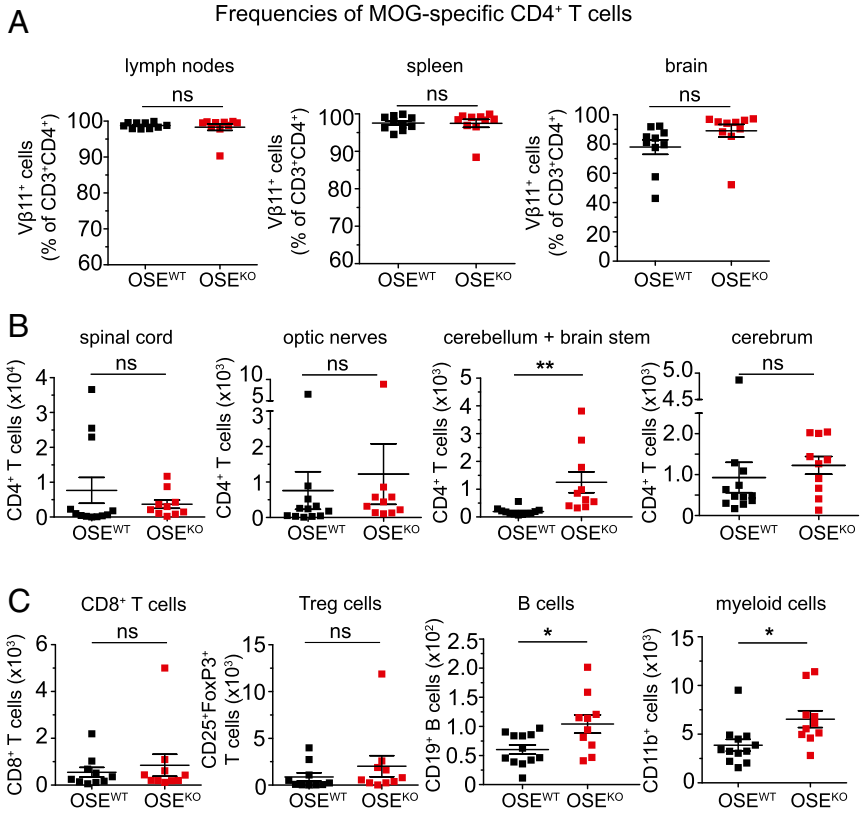

Fig. 2. B7-H1 limits T-cell infiltration in the cerebellum and brainstem of OSE mice at disease onset. (*A*) Frequencies of MOG-specific $CD4^+$ T cells (percent of $CD3^+CD4^+$) in the lymph nodes, spleen, and brain, as determined by flow cytometry. (*B*) Absolute numbers of $CD4^+$ T cells in different CNS regions of OSE^{WT} and OSE^{KO} mice at disease onset (mean age 28 d), as determined by flow cytometry and using cell-counting beads. (*C*) Absolute numbers of immune cells (as indicated) in the cerebellum and brainstem of OSE^{WT} and OSE^{KO} mice at disease onset (mean age 32 d), determined by flow cytometry and using cell-counting beads. Each data point represents one mouse. Unpaired, two-tailed Student's *t* test. $*P < 0.05$; $**P < 0.01$; ns, not significant.

interaction with either $B7\text{-}H1^{WT}$ or $B7\text{-}H1^{KO}$ T cells was not differentially affected (Fig. S4*E*). In contrast, activated $B7\text{-}H1^{KO}$ T cells produced significantly increased numbers of cytotoxic molecules, such as granzyme A and granzyme B, compared with WT T cells (Fig. 4*I*). Taken together, lack of B7-H1 on T cells results in enhanced proinflammatory and lytic effector functions such as IFN-γ and granzyme A and B production upon T-cell activation.

Lack of B7-H1 on T Cells Augments Their Capacity to Elicit Brain Endothelial Barrier Dysfunction and Increased Permeability. After having demonstrated that lack of B7-H1 doesn't alter peripheral T-cell polarization but increases T-cell effector functions, we asked whether $B7\text{-}H1^{KO}$ T cells might exhibit an enhanced capacity to penetrate the endothelial barrier compared with B7-H1–competent T cells. To this end, we investigated whether B7-H1 ablation on T cells affects mouse brain microvascular endothelial cell (MBMEC) barrier properties upon coculture of brain endothelial cells with T cells by assessing changes in transendothelial electrical resistance (TEER). First, TEER was not affected upon interaction of naive $CD4^+$ T cells with brain endothelial cells. Activated T cells, however, exhibited a distinct capacity to affect barrier integrity, as reflected by a significant decrease in TEER (Fig. 5*A*). Importantly, this drop in TEER was significantly more pronounced upon interaction with $B7\text{-}H1^{KO}$ T cells (Fig. 5*A*), which was associated with a persistent increase in capacitance (Fig. 5*A*), as well as enhanced MBMEC monolayer permeability to small (dextran-fluorescein) as well as larger molecules (dextran-Texas Red) (Fig. 5*B*), thus illustrating a relevant decrease in endothelial barrier integrity. Further experiments revealed that T-cell–endothelial cell contact is required and decisive for this effect because supernatants derived from activated $CD4^+$ T cells were not sufficient to affect TEER and capacitance in this setup (Fig. 5*C*). Delivery of a strong immune-inhibitory signal to activated $CD4^+$ T cells via use of a B7-H1–Ig fusion protein (16) was capable of abrogating T-cell–mediated disturbance of endothelial barrier integrity (Fig. 5*D*), suggesting that the strength of T-cell activation, shaped by the balance between costimulatory and coinhibitory signals, directly influences their capacity to impair endothelial barrier function upon contact.

Further experiments revealed that neutralization of IFN-γ was partially effective in restoring TEER upon interaction with activated $CD4^+$ T cells. This restoration was even less pronounced using $B7\text{-}H1^{KO}$ T cells (Fig. 5*E*), indicating that IFN-γ is involved but doesn't act as the crucial part of T-cell–mediated endothelial cell dysfunction. In sharp contrast, interference with granzyme function using granzyme B inhibitor II was capable of completely restoring TEER in the presence of both WT and $B7\text{-}H1^{KO}$ T cells (Fig. 5*F* and Fig. S5*B*), indicating that these activated T cells indeed elicit endothelial barrier dysfunction via granzyme-mediated, cell contact-dependent endothelial barrier damage in vitro. Following this line, we wanted to further address the link between granzyme B production by activated $CD4^+$ T cells and endothelial cell damage by performing coculture assays of preactivated $CD4^+$ T cells and MBMECs. Interestingly, granzyme B production by $CD4^+$ T cells was significantly enhanced upon coculture with brain endothelial cells, and this increase was much more pronounced in $2D2^{KO}$ T cells compared with $2D2^{WT}$ T cells (Fig. 5*G*). What is more, $2D2^{KO}$ T cells displayed a greater capacity to elicit endothelial cell death than $2D2^{KO}$ T cells, and this difference was completely abrogated in the presence of granzyme B inhibitor II (Fig. 5*H*). These data indicate

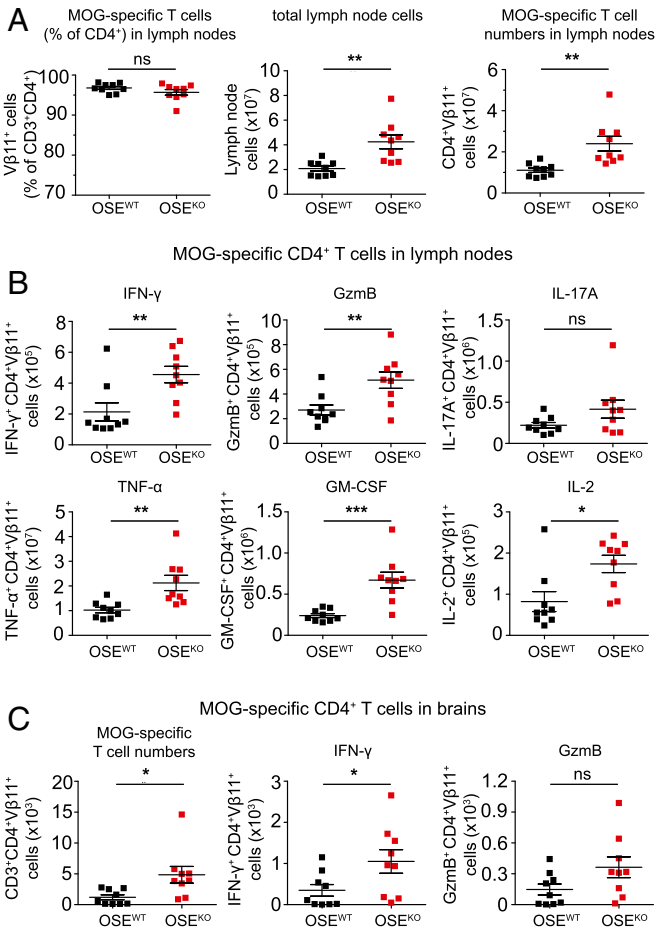

Fig. 3. B7-H1 inhibits expansion of cytokine-producing MOG-specific CD4$^+$ T cells in lymph nodes and brains of sick OSE mice. (*A*) Frequencies and numbers of MOG-specific CD4$^+$ T cells in lymph nodes of OSE^{WT} and OSE^{KO} mice with established disease (score-matched, mean clinical score 4) were analyzed. (*Left*) Frequencies of MOG-specific CD4$^+$ T cells in lymph nodes, as determined by flow cytometry. (*Center*) Absolute cell numbers of total lymph nodes as determined by Neubauer cell-counting chamber. (*Right*) Absolute numbers of MOG-specific CD4$^+$ T cells within total lymph nodes as determined by flow cytometry. (*B* and *C*) Flow cytometric analysis of MOG-specific CD4$^+$ T cells producing effector molecules in total lymph nodes (*B*) and brains (*C*) of sick OSE mice (as described in *A*), after 4 h of ex vivo restimulation with PMA and ionomycin. Absolute numbers of brain-derived MOG-specific CD4$^+$ T cells (*C*, *Left*), as well as numbers of IFN-γ and GzmB producing MOG-specific T cells (*Center* and *Right*). Each data point represents one mouse. Unpaired, two-tailed Student's *t* test. *$P < 0.05$; **$P < 0.01$; ***$P < 0.001$; ns, not significant.

that, indeed, activated CD4$^+$ T cells can produce functionally relevant amounts of granzyme B—especially in the presence of endothelial cells—to cause EC death and that this production is modulated by B7-H1 on T cells.

Lack of B7-H1 in OSE Mice Is Associated with Increased BBB Permeability in Supratentorial Brain Regions in Vivo. Finally, we aimed to address whether B7-H1^{KO} T cells preferentially cause blood–brain barrier breakdown in certain topographical regions: namely, supratentorial brain regions in the context of spontaneous CNS autoimmunity in vivo. We therefore evaluated blood–brain barrier integrity in 10 score-matched mice (mean score of 6) by assessing Evans Blue leakage from microvessels after intravenous injection into living mice. Indeed, whereas all animals displayed comparable Evans Blue leakage in the spinal cord, reflecting the predominance of spinal cord inflammation in this animal model, 9 out of 10 OSE^{KO} mice, but only 3 out of 10 OSE^{WT} mice, displayed Evans Blue leakage in supratentorial brain areas, especially the periventricular region (Fig. 5*I*), which further supports the notion of changes in regional encephalitogenicity of T cells lacking immune-regulatory B7-H1, thus strongly contributing to the altered lesion distribution and dissemination of CNS autoinflammation.

Discussion

Using a model system of spontaneous CNS autoimmunity, our study provides evidence that genetic deficiency of a single immune-regulatory molecule (i.e., B7-H1) in autoimmune-susceptible hosts can determine substantial changes in lesion topography critically influenced by regional breaching of the blood–brain barrier. In light of its relevance for maintenance of immune tolerance, the role of B7-H1 on APCs has been addressed in CNS autoimmunity before: In active $MOG_{35–55}$-induced EAE, B7-H1 knock-out resulted in an enhanced disease severity, which was linked to B7-H1 expressed on APCs (18). Moreover, enhanced expression of B7-H1 was observed in MS lesions and attributed to macrophages/microglial cells, as well as astrocytes (18, 19). In the periphery, B7-H1 expression has been analyzed on B cells and monocytes from MS patients; here, an increased percentage of B7-H1–positive cells was found in stable versus active MS patients (20). In contrast to these studies, however, the relevance of B7-H1 on T cells has not been studied in the context of MS so far.

The advent of novel transgenic mouse models featuring spontaneous development of CNS inflammation offers the unique opportunity to study the very first steps in immune cell activation and lesion development (21, 22). This model is in contrast to conventional EAE models, where exogenous application of microbial adjuvants is indispensable for disease induction, which is known to affect the mechanisms of (auto-) immune cell activation and BBB permeability. Several hallmarks of the double-transgenic OSE mouse model used in our study deserve attention. First, autoreactive T-cell activation is triggered by MOG-presenting B cells serving as the main source of professional APCs in this particular animal model (3). Second, T-cell responses in these mice are predominantly of a T_H1 phenotype, with a minor role of IL-17A production (3, 15). And, third, inflammatory demyelinating CNS lesions are confined to the spinal cord and optic nerves, but not the brain, brainstem, or cerebellum (3, 15). With regard to the first aspect, we addressed the impact of lack of B7-H1 on either APCs or CD4$^+$ T cells by performing coculture assays of MOG-specific B cells and MOG-specific CD4$^+$ T cells in the presence of recombinant MOG protein and observed that B7-H1 was completely dispensable on antigen-presenting B cells but augmented CD4$^+$ T-cell expansion and effector functions when lacking on the T-cell side. The B7-H1–PD-1 pathway has received major attention over the last years as a key component of the B7-homologs involved in the regulation of immune tolerance, tumor surveillance, and autoimmunity (18, 23–25). Despite its well-known role in immune regulation by APCs via interaction with its canonical receptor PD-1 on T cells, only a few studies so far have investigated the relevance of B7-H1 on T cells: Talay et al. observed that expression of B7-H1 was required for T-cell–mediated conditioning of dendritic cell maturation in the context of infections (26). However, when evaluating classical maturation markers of APCs, such as expression of costimulatory molecules, we did not observe any difference in expression levels, at least in vitro. Another publication described *in trans* control of T_H17 differentiation via B7-H1 expression on adjacent CD4$^+$ T cells (27). In contrast to these findings, we did not observe a particular increase in T_H17 responses due to lack of B7-H1 on T cells, either in vitro or in vivo. Instead, we here provide evidence that lack of B7-H1 on T cells boosts their expansion in vitro and promotes particular effector functions, such as production of IFN-γ and granzyme A and B. The interaction partner of B7-H1 expressed on T cells, however, remains unclear because both PD-1 and CD80 do not seem to be critically involved (Figs. S4*C* and S5*A*), which is in line with a previous publication by our group (16) and

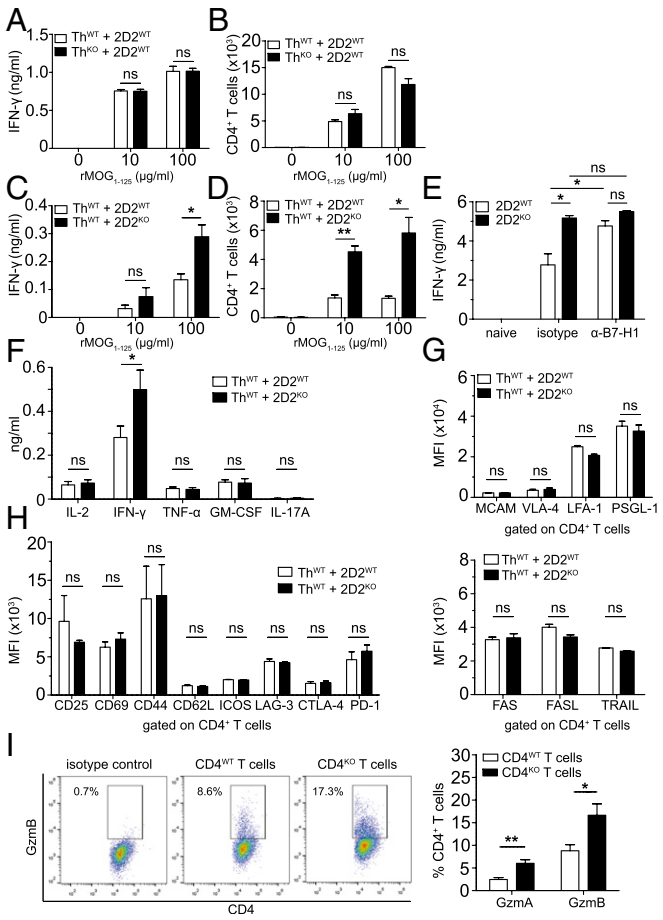

Fig. 4. B7-H1 on MOG-specific T cells, but not on MOG-specific B cells, limits antigen-specific T-cell activation. (*A* and *B*) Coculture of MOG-specific 2D2 T cells and MOG-specific antigen-presenting Th B cells in the presence or absence of recombinant $MOG_{1–125}$ protein for 4 d; antigen-presenting B cells either express B7-H1 (Th^{WT}) or lack B7-H1 (Th^{KO}). (*A*) IFN-γ production as determined by ELISA. (*B*) T-cell expansion at the end of coculture as determined by flow cytometry using cell-counting beads. (*C* and *D*) Coculture of MOG-specific 2D2 T cells and MOG-specific antigen-presenting Th B cells in the presence or absence of recombinant $MOG_{1–125}$ protein for 4 d; antigen-specific T cells either express B7-H1 ($2D2^{WT}$) or lack B7-H1 ($2D2^{KO}$) (analysis as described above). (*E*) IFN-γ production (ELISA) by MOG-specific $2D2^{WT}$ or $2D2^{KO}$ $CD4^+$ T cells after stimulation with precoated α-CD3 and soluble α-CD28 (both at 1 μg/mL) for 3 d in the presence of a blocking α-mouse B7-H1 antibody (added at 40 μg/mL each day) or the corresponding isotype control. (*F–H*) Cytokine production and expression of various T-cell markers on $2D2^{WT}$ and $2D2^{KO}$ T cells after coculture with Th^{WT} B cells in the presence of $MOG_{35–55}$ (20 μg/mL). (*F*) Cytokine production was analyzed after 5 d. (*G*) Expression levels of cell adhesion molecules and (*H*) T-cell activation markers, costimulatory and coinhibitory molecules, and apoptosis-inducing molecules on $CD4^+$ T cells were analyzed by flow cytometry after 3 d (except for CD69—after 1 d). (*I*) Flow cytometric analysis of granzyme A- and granzyme B-producing $CD4^{WT}$ and $CD4^{KO}$ T cells. T cells were polyclonally stimulated with precoated α-CD3 and soluble α-CD28 (both at 1 μg/mL) for 2 d. (*A–D*) Results show technical triplicates and are representative of five independent experiments for each set-up. (*E*) Data show one representative experiment (five mice per genotype) out of three independent experiments. (*F*) Supernatants from at least nine coculture experiments were used (except for GM-CSF—from five coculture experiments). (*G* and *H*) Pooled results from at least two independent experiments. (*I*) Five mice per genotype were used. Unpaired, two-tailed Student's *t* test. $*P < 0.05$; $**P < 0.01$; ns, not significant.

which argues in favor of a novel yet unknown receptor for B7-H1, as has also been proposed by other groups (28, 29).

Ultimately, we cannot rule out that, in our in vivo model during spontaneous CNS autoimmunity, lack of B7-H1 on non-T cells might additionally contribute to the overall phenotype of these mice. There are nonetheless several arguments that argue against a strong relevance of such a contribution in our model. Despite accumulation of MOG-specific $CD4^+$ T cells in the periphery, we did not observe an increase in the percentages of cytokine-producing $CD4^+$ T cells, both in lymph nodes and within the CNS of sick OSE^{KO} vs. OSE^{WT} mice, indicating that cytokine production on a per cell basis is not affected in these animals (Fig. S3). Moreover, absolute numbers of cytokine-producing $CD4^+$ T cells were unaffected within the classical predilection sites of inflammatory CNS lesions in this animal model: i.e., spinal cord and optic nerves. Instead, we observed T-cell infiltrates in brain areas of OSE^{KO} mice that are classically spared in this model, such as brainstem, cerebellum, and cerebrum, especially in the corpus callosum and periventricular regions, which at least suggests that these T cells acquired functions that are distinct from the functions of T cells derived from OSE^{WT} mice. Further analysis of these brain infiltrates by histology and flow cytometry, respectively, revealed that these lesions predominantly consisted of MOG-specific effector $CD4^+$ T cells, and we did not find significant numbers of $CD8^+$ T cells or altered frequencies of $FoxP3^+$ regulatory T cells within these infiltrates.

Several factors have been discussed to determine lesion distribution in CNS inflammation and might favor nonspinal manifestation of disease. First, the density of antigen expression in different target (CNS) areas, in conjunction with the antigen specificity of CNS-autoreactive T cells, has been suggested to influence lesion topography (3–5). However, in light of the particular animal model used in our study, we can exclude variations of antigen density or T-cell antigen specificity contributing to the observed changes in lesion topography. Second, T helper-cell polarization, especially the ratio between autoreactive T_H1 and T_H17 cells, has been shown to determine lesion topography in different animal models (6, 7, 30), with T_H1 cells favoring typical spinal disease manifestation and T_H17 cells rather favoring cerebellar and supratentorial lesion development. However, as also described before, we observed a strong predominance of T_H1 responses in the OSE animal model, and, more importantly, this predominance was preserved upon additional lack of B7-H1, thus ruling out that atypical lesion topography in these mice might be associated with a preponderance of T_H17 responses. Along these lines, it has been proposed that T_H17 cells can serve as gatekeepers of other T cells by entering the CNS via the choroid plexus in a CCR6-dependent fashion; however, the authors of that study did not make use of a spontaneous model of CNS autoimmunity (8). We therefore investigated the potential entry route of these brain-infiltrating T cells in sick OSE^{KO} mice and observed that most T-cell infiltrates were located around perivascular areas whereas leptomeningeal T cells and T cells in the choroid plexus were scarcely present. These histological findings nicely correlated with focal breakdown of the BBB in these areas, confined to OSE^{KO} mice but not OSE^{WT} mice, as demonstrated by our Evans Blue leakage experiments in score-matched mice. Of note, also in these leakage experiments, the difference in blood–brain barrier breakdown was confined to the brain, especially in the periventricular areas, whereas leakage in the spinal cord was not altered in OSE^{KO} mice. Following this line, our in vitro experiments using MOG-specific $B7\text{-}H1^{KO}$ T cells vs. $B7\text{-}H1^{WT}$ T cells clearly demonstrate that B7-H1 expression on T cells determines their capacity to affect BBB integrity as reflected by the extent of TEER drop upon direct contact of T cells with primary brain endothelial cells. These data thus indicate that expression of B7-H1 on T cells is decisive for the extent of certain T-cell effector functions, especially IFN-γ and granzyme production, which in turn might affect their capacity to inflict local BBB dysfunction.

From a more general point of view, our data reveal that the activation status of encephalitogenic $CD4^+$ T cells directly influences their capacity to evoke BBB dysfunction. This hypothesis is

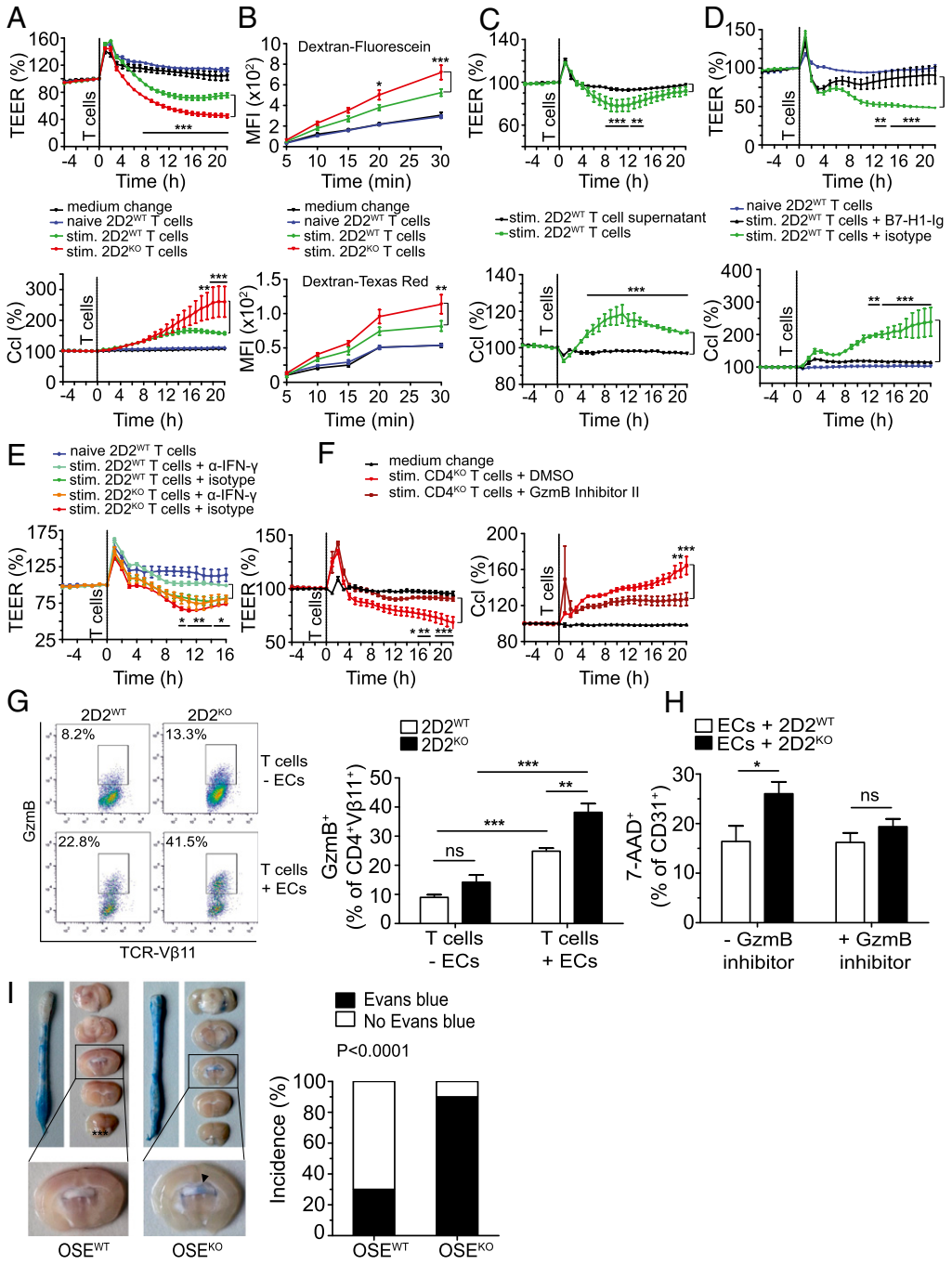

Fig. 5. B7-H1 on CD4$^+$ T cells restricts T-cell–mediated brain endothelial cell dysfunction, at least partly via inhibition of granzyme B function, and limits cerebral BBB permeability in vivo. (*A* and *C*–*F*) TEER measurements were performed by coculturing MBMECs (2×10^4 per well) with T cells (0.2×10^6 per well), their supernatants, or α–IFN-γ antibody, as indicated; TEER and Ccl were measured every hour for 1 d. (*A*) TEER measurement with 2D2^{WT} or 2D2^{KO} T cells, naive or preactivated by Th^{WT} B cells and $MOG_{35–55}$ (20 μg/mL) for 5 d. (*B*) Permeability of MBMECs to dextran-fluorescein and dextran-Texas Red using samples from *A* after TEER measurement. (*C*) TEER measurement with stimulated 2D2^{WT} T cells or their supernatants. T cells were preactivated as in *A*. (*D*) TEER measurement with 2D2^{WT} T cells, preactivated with precoated α-CD3 and soluble α-CD28 (both 1 μg/mL), in the presence of B7-H1–Ig fusion protein (10 μg/mL) or the corresponding isotype control, for 2 d. (*E*) TEER measurement with MOG-activated 2D2^{WT} or 2D2^{KO} T cells, in the presence of neutralizing α-IFN-γ antibody (20 μg/mL) or the corresponding isotype control, during the coculture of T cells and MBMECs. (*F*) TEER measurement with CD4^{KO} T cells, preactivated as in *D* in the presence of granzyme B inhibitor II (10 μM) or its diluent DMSO. (*G*) Flow cytometric analysis of GzmB production by 2D2^{WT} or 2D2^{KO} T cells (%), alone or cocultured with MBMECs. T cells were stimulated with precoated α-CD3 and soluble α-CD28 (both at 1 μg/mL) for 3 d. Next, T cells were harvested and cultured either alone or with MBMECs for another 24 h. (*H*) Flow cytometric analysis of 7-AAD$^+$ CD31$^+$ MBMECs after 24 h of coculture with 2D2^{WT} or 2D2^{KO} T cells (stimulated as in *G*). T cells were cultured in the presence of GzmB inhibitor II (10 μM) or DMSO, added at the beginning of T-cell stimulation. (*I*) BBB leakage in brains and spinal cords of score-matched OSE^{WT} and OSE^{KO} mice ($n = 10$; mean clinical score 6), as visualized by Evans Blue dye. (*I*, *Right*) Incidence of mice (%) with Evans Blue leakage in the supratentorial brain regions. (*A*–*E*) Results show technical triplicates and are representative of three independent experiments each. (*F*) Results show three biological replicates and are representative of two independent experiments. (*G* and *H*) Five mice per genotype were used for each setup. (*A*–*F*) Two-way ANOVA with Bonferroni correction for multiple comparisons. (*G* and *H*) Unpaired, two-tailed Student's *t* test. (*I*) Fisher's exact test. $^*P < 0.05$; $^{**}P < 0.01$; $^{***}P < 0.001$; ns, not significant.

supported by several datasets here: (*i*) Naive $CD4^+$ T cells did not affect BBB function at all in comparison with activated $CD4^+$ T cells; (*ii*) B7-$H1^{KO}$ T-cell–induced BBB dysfunction was much more pronounced than B7-$H1^{WT}$ T-cell–induced dysfunction, as reflected by TEER measurement as well as our permeability assays; and (*iii*) inhibition of T-cell activation via delivery of a soluble B7-H1–Ig molecule profoundly restricted their capacity to elicit BBB dysfunction (16). Although an impact of immune cells on BBB integrity in the context of CNS autoimmunity is conceivable, very few publications so far have addressed direct T-cell–mediated influence on BBB integrity: Kebir et al. demonstrated that human T_H17 cells preferentially promote BBB disruption compared with human T_H1 cells (31), and Huppert et al. provided additional evidence that IL-17A is critically involved in such immune cell-mediated endothelial barrier dysfunction (32). Our system didn't study specifically T_H17 cells, and IL-17A seems not to be a critical player for endothelial dysfunction: we did not observe that activated MOG-reactive $CD4^+$ T cells produced substantial amounts of IL-17A, at least in vitro, and, moreover, lack of B7-H1 did enhance T-cell–mediated BBB dysfunction despite similar IL-17A production by these cells. Additionally, at least in our hands, soluble factors, such as proinflammatory cytokines, seem to play only a minor role because supernatants from highly activated T cells were not sufficient to induce relevant BBB dysfunction, in stark contrast to direct interaction of activated T cells and brain endothelial cells. However, it should be pointed out that Kebir et al. (31) described pronounced granzyme B expression by these human T_H17 cells. Although they did not investigate whether granzyme B was involved in T_H17-mediated endothelial dysfunction, they described pronounced T_H17-mediated killing of primary neurons.

We now extend these findings as we provide clear evidence of $CD4^+$ T-cell–mediated BBB dysfunction, independent from IL-17A, that is cell contact-dependent and at least partly depends on granzyme B expression by these T cells because the granzyme B inhibitor II profoundly ameliorated T-cell–mediated BBB dysfunction by both B7-$H1^{KO}$ T cells and B7-$H1^{WT}$ T cells. Following this line, we could show that, at least in vitro, brain endothelial cells enhance granzyme B production by activated $CD4^+$ T cells and that activated B7-$H1^{KO}$ T cells elicit brain endothelial cell death upon coculture in a granzyme B-dependent fashion. Interestingly, granzyme release has already been implicated in the context of immune cell transmigration across endothelial cells—including $CD4^+$ T cells—albeit not in the context of multiple sclerosis (33). Mechanistically, such granzyme release by T cells has been linked to endothelial cell apoptosis in vivo in mouse models of atherosclerosis and transplant vascular disease (34, 35). The functional relevance of granzyme B production in T-cell–mediated myocarditis was also suggested by demonstration of a link between reduced granzyme expression and reduced myocardial injury upon antiinflammatory intervention (36). In human cases of T-cell–mediated skin eruptions, there was a strong correlation between granzyme expression and endothelial cell apoptosis (37). Together, these findings imply a link between granzyme released by effector T cells, endothelial cell apoptosis, and immune cell transmigration in vivo.

What is the relevance of our findings with regard to the understanding of human CNS autoimmunity? We here provide a proof-of-concept that subtle alterations in T-cell function caused by dysregulation of single immune-regulatory molecules might explain interindividual, as well as intraindividual, changes in lesion topography and phenotypes of MS. One plausible cause for such interindividual variations could be the presence of single nucleotide polymorphisms in immune-relevant genes in individuals (38). On the other hand, especially, intraindividual changes might be caused as bystander effects due to altered expression of costimulatory or coinhibitory molecules in the context of bacterial or viral infections (39, 40). Following this line, such changes in expression levels of immune-regulatory molecules or adhesion molecules with their consequences with regard to T-cell invasion into the CNS might also account for so far unexplained decreases in the individual treatment response during the course of therapy, as observed in the context of natalizumab treatment. In this context, it is important to note that the B7-H1/PD-1 pathway is obviously key to susceptibility and disease type/course of several autoimmune disorders, including MS (41–43), which puts our findings into the overriding context of what functional consequences certain risk genes can have. This study demonstrates that single immune regulatory molecules affecting the activation status of (encephalitogenic) T cells can influence lesion distribution, which is associated with an altered capacity of these cells to elicit transient focal EC dysfunction and barrier dysfunction as essential steps for lesion development.

Finally, these findings imply that therapeutic options specifically targeting the expression level and/or function of single immune-regulatory molecules on $CD4^+$ T cells might selectively affect their capacity to compromise BBB integrity without impairing their capacity for immune surveillance under homeostatic conditions, as observed in the context of drugs interfering with immune cell trafficking (44). The feasibility of such an approach could be illustrated by our experiment, using a soluble B7-H1–Ig molecule interfering with activation of $CD4^+$ T cells, that profoundly diminished their capacity to impair BBB integrity.

Materials and Methods

Detailed methods are provided in *SI Materials and Methods*.

Animals. C57BL/6 mice were purchased from Harlan Laboratories. Transgenic lines were on a C57BL/6 background and were purchased from The Jackson Laboratory. B7-$H1^{KO}$ mice (45) were provided by L. Chen, Johns Hopkins University School of Medicine, Baltimore. Th (IgH^{MOG}) mice (46) were crossed to 2D2 (TCR^{MOG}) mice (47) to create OSE^{WT} mice (opticospinal EAE, also referred to as Devic), as previously described (3). Th B7-$H1^{KO}$ mice were crossed to 2D2 B7-$H1^{KO}$ mice to create OSE^{KO} mice. For all experiments, mice were bred and maintained under specific pathogen-free conditions in the central animal facility at the University of Münster, according to German guidelines for animal care. All experiments were performed according to guidelines of the animal experimental ethics committee and approved by the local authorities of North Rhine-Westphalia, Germany.

Spontaneous EAE Incidence, Disease Severity, and Survival of OSE Mice. OSE^{WT} and OSE^{KO} mice were monitored daily for the presence and severity of EAE symptoms. Disease severity was determined on a scale from 0 to 8: 0, healthy; 1, limp tail; 2, ataxia or unilateral hindlimb paralysis; 3, moderate unilateral or mild bilateral hindlimb paralysis; 4, moderate bilateral hindlimb paralysis; 5, complete hindlimb paralysis; 6, complete hindlimb and partial forelimb paralysis; 7, complete quadriplegia; 8, moribund. Mice with a score of 6 or higher were immediately taken out of the experiment and euthanized. Accordingly, for analysis of survival of OSE^{WT} and OSE^{KO} mice, a death event was recorded when a clinical score of at least 5.5 was reached. Mice eliminated for reasons unrelated to disease severity were recorded as censored (all with a score of less than 5.5) and were also included in the survival analysis.

Immunohistochemistry. Score-matched OSE^{WT} and OSE^{KO} mice (mean clinical score 5.75) were killed under deep anesthesia and transcardially perfused with PBS and 4% (wt/vol) paraformaldehyde (PFA) in PBS. Spleen, spinal cords, and brains were dissected and fixed in 4% (wt/vol) PFA overnight. Two days later, 4% (wt/vol) PFA was removed, and the CNS tissue was kept in PBS at 4 °C until further processing. The brain was cut into three coronar sections whereas the cervical, thoracic, and higher lumbar spinal cord was cut into 8–11 3-mm-thick transverse segments before embedding. To perform semiquantitative analysis of infiltrates in cerebrum and brainstem, the brain was sagitally cut in the midline. Five-micrometer-thick sections were stained for hematoxylin/eosin and Luxol-fast blue (LFB)/periodic acid-Schiff (PAS). To detect macrophages/microglia, immunohistochemistry was performed using a biotin-streptavidin peroxidase technique (K5001; Dako) and an automated immunostainer (AutostainerLink 48; Dako). Sections were pretreated in a steamer (treatment solutions pH 6.0 or 9.0; Dako) before incubation with the primary antibodies anti-Mac3, (clone M3/84, 553322, 1:100; BD Pharmingen), α-CD3 (MCA 1477, 1:50; Serotec), or α-CD8 (clone C8/144B, 1:100; Dako). DAB was used as a chromogen, and sections were counterstained using hematoxylin.

Preparation of CNS Mononuclear Cells. For flow cytometric analysis of immune cell infiltration in the CNS, mononuclear cells were isolated as previously described (48). Briefly, anesthetized mice were transcardially perfused with 20 mL of PBS, and CNS tissue was removed, homogenized with scissors, and digested with Collagenase Type IA (0.4 mg/mL; Sigma Aldrich) for 30 min in a water bath at 37 °C. Digested tissue was passed through a cell strainer and extensively washed before Percoll density centrifugation. Mononuclear cells were collected from the interphase of the discontinuous Percoll gradient, washed twice with PBS containing 1% FCS, and resuspended in FACS buffer for flow cytometry.

B- and T-cell Isolation and Culture. For ex vivo analysis of lymph node-derived T cells from OSE mice, the following lymph nodes were used: inguinal, brachial, axillary, and cervical (referred to as total lymph nodes). For in vitro studies of cytokine production and proliferation of T cells activated by B cells, cocultures of B and T cells were set up as follows: B cells from spleens of Th or Th B7-H1^{KO} mice were isolated using CD19 MACS MicroBeads (Miltenyi). Cells were resuspended in B-cell medium, containing X-VIVO 15 medium (Lonza), 10% (vol/vol) FCS, 1% penicillin/streptavidin (Sigma Aldrich), 1% L-glutamine, and 50 μM β-mercaptoethanol (Gibco). Recombinant mouse $MOG_{1–125}$ protein (AnaSpec) was incubated with B cells (5×10^6 in 500 μL total volume) for 30 min on ice; cells were then washed with PBS (Sigma Aldrich) and incubated in 1 mL of B-cell medium at 37 °C for 2 h. CD4$^+$ T cells from spleens and lymph nodes of 2D2 or 2D2 B7-H1^{KO} mice were isolated using CD4 MACS MicroBeads (Miltenyi). For isolation of MOG-specific CD4$^+$ T cells (Figs. 4*E* and 5 *G* and *H* and Figs. S4 *A–C* and S5*A*), biotinylated α-mouse TCR-Vβ11 antibody (clone RR3-15; BD Biosciences) was used (at 10 μg/mL), which was followed by MACS separation with α-biotin MicroBeads (Miltenyi). B and T cells were seeded onto a round-bottom 96-well plate at a 1:1 ratio (0.1×10^6 each). For TEER measurements, $MOG_{35–55}$ (Biotrend) at 20 μg/mL was used instead of $rMOG_{1–125}$ protein. B and T cells were cocultured for 4 to 5 d at a 1:2 ratio (0.05×10^6 B and 0.1×10^6 T cells per well).

Flow Cytometry. For the detection of cell surface markers, single-cell suspensions were stained with fluorochrome-conjugated anti-mouse monoclonal antibodies (mAbs) or the appropriate isotype controls in FACS buffer (PBS, 1% FCS, 2 mM EDTA, 0.1% NaN_3) for 30 min at 4 °C, protected from light. For intracellular cytokine staining, cells were first stimulated for 4 h at 37 °C with phorbol 12-myristate 13-acetate (PMA) (0.25 ng/μL) and ionomycin (0.4 ng/mL) (both from Sigma Aldrich), in the presence of GolgiPlug (1 μL/mL; BD Pharmingen). Next, cells were stained for cell surface markers, fixed, and permeabilized using Cytofix/Cytoperm and Perm/Wash buffer (BD Biosciences) according to the manufacturer's instructions and stained for intracellular cell markers. CountBright absolute counting beads (Life Technologies) were used to determine absolute numbers of proliferated T cells, according to the manufacturer's instructions. Measurements were performed on a Gallios flow cytometer (Beckman Coulter), and analysis was done using FlowJo7.6.5 software (Tree Star).

ELISA. Cytokine production by CD4$^+$ T cells activated by B cells in the presence of MOG (as described above) was determined by mouse ELISA Ready-Set-Go! kit (eBioscience) according to the manufacturer's instructions. The kits were used for the following cytokines: IL-2, IFN-γ, IL-17A, TNF-α, and GM-CSF. OD values of supernatants were measured with a microplate reader (Thermo) at 450 nm, and wells with only B-cell medium were used as blank. Supernatants from cocultures with naive CD4$^+$ T cells (cocultures without MOG) were used as negative controls.

MBMEC Isolation and Culture. MBMECs were isolated as previously described (49–51). After isolation, cells were cultured at 37 °C, 5% CO_2, and fresh MBMEC medium without Puromycin was added after 4 d. The next day, when the cells reached confluence, they were trypsinized, washed, and counted for subsequent TEER experiments.

For flow cytometric analysis of cocultures of MBMECs and T cells, MBMECs were cultured on a precoated flat-bottom 96-well plate. When confluence was reached, MOG-specific CD4$^+$ T cells from 2D2^{WT} or 2D2^{KO} mice (prestimulated for 2 d with α-CD3/CD28, both at 1 μg/mL) were added to MBMECs (0.1×10^6 T cells per well); 24 h later, MBMECs and T cells were harvested by trypsinization, washed, and analyzed by flow cytometry.

TEER Measurement. Five days after isolation, MBMECs were trypsinized, resuspended in MBMEC medium, and seeded onto precoated Transwell inserts (pore size 0.4 μm; Corning) at 2×10^4 cells per insert, and placed in cellZscope. TEER measurements were performed using the cellZscope 24-cell module and cellZscope v2.2.2 Software (nanoAnalytics GmbH) essentially as described before (52). Automated TEER and Ccl measurements were made every hour for 4 to 5 d until the cell monolayer reached full confluence, as determined by stable Ccl at 0.7 μF/cm^2 and TEER at its maximum level for at least a few hours. Next, MBMECs were treated with preactivated MOG-specific CD4$^+$ T cells or their supernatants. Then, 0.2×10^6 T cells per insert were added directly on top of MBMECs, and the measurement was resumed for another 24 h. Acquired data were exported and analyzed using GraphPad Prism 5 software.

Permeability Assay. Permeability assays were performed as previously described (52, 53), with certain modifications. Fluorescently labeled dextran conjugates fluorescein (3 kDa) and Texas Red (70 kDa) (both from Molecular Probes) were added at 0.1% in Hepes buffer on top of each insert and let to diffuse through the MBMEC monolayer. After indicated time points, flow-through was collected from the lower compartment and transferred to a black 96-well plate. An Infinite M200 PRO Tecan plate reader was used to measure fluorescence intensity (fluorescein, excitation 494 nm, emission 521 nm; Texas Red, excitation 595 nm, emission 625 nm). Wells with only Hepes buffer served as blank.

In Vivo BBB Permeability Assay. For visualization of the BBB leakage in sick OSE^{WT} and OSE^{KO} mice, Evans Blue dye was used as described (52), with certain modifications. One-hundred microliters of 2% (wt/vol) Evans Blue (Sigma Aldrich) in PBS was injected intravenously into the tail vein of score-matched (mean score 6) OSE^{WT} and OSE^{KO} mice. One hour later, mice were killed and transcardially perfused with 20 mL of PBS. The spinal cord and brain were dissected, and 2-mm-thick brain sections were made using acrylic brain matrix (World Precision Instruments), photographed, and assessed for the presence of the dye in the supratentorial brain areas.

Statistical Analysis. All statistical tests were performed using GraphPad Prism 5 software. Values are presented as mean ± SEM. For the analysis of survival of OSE^{WT} and OSE^{KO} mice and EAE incidence, a log-rank (Mantel–Cox) test was used. Two-way ANOVA with Bonferroni correction for multiple comparisons was used for analysis of clinical scores of OSE mice, TEER measurements, and permeability assays. Fisher's exact test was used for the analysis of contingency tables, as indicated. An unpaired, two-tailed Student's *t* test was used for comparisons of means between two groups ($*P < 0.05$; $**P < 0.01$; $***P < 0.001$; ns, not significant).

ACKNOWLEDGMENTS. We thank Annika Engbers, Andrea Pabst, Frank Kurth, and Claudia Kemming for excellent technical support. This work was supported by DFG SFB1009 Project A03 (to H.W. and L.K.); CRC TR128 Projects A08, Z1, and B01 (to L.K., T.K., and H.W.); and Interdisciplinary Center for Clinical Research (Medical Faculty of Münster) Grant Kl2/2015/14 (to L.K.).

1. Bennett JL, Stüve O (2009) Update on inflammation, neurodegeneration, and immunoregulation in multiple sclerosis: Therapeutic implications. *Clin Neuropharmacol* 32(3):121–132.
2. Lassmann H (1998) The pathology of multiple sclerosis. *McAlpine's Multiple Sclerosis*, ed Alastair C (Churchill Livingstone, Hong Kong), 3rd Ed, pp 323–358.
3. Krishnamoorthy G, Lassmann H, Wekerle H, Holz A (2006) Spontaneous opticospinal encephalomyelitis in a double-transgenic mouse model of autoimmune T cell/B cell cooperation. *J Clin Invest* 116(9):2385–2392.
4. Berger T, et al. (1997) Experimental autoimmune encephalomyelitis: The antigen specificity of T lymphocytes determines the topography of lesions in the central and peripheral nervous system. *Lab Invest* 76(3):355–364.
5. Fukazawa T, et al. (2000) Both the HLA-CPB1 and -DRB1 alleles correlate with risk for multiple sclerosis in Japanese: Clinical phenotypes and gender as important factors. *Tissue Antigens* 55(3):199–205.
6. Stromnes IM, Cerretti LM, Liggitt D, Harris RA, Goverman JM (2008) Differential regulation of central nervous system autoimmunity by T(H)1 and T(H)17 cells. *Nat Med* 14(3):337–342.
7. Rothhammer V, et al. (2011) Th17 lymphocytes traffic to the central nervous system independently of α4 integrin expression during EAE. *J Exp Med* 208(12):2465–2476.
8. Reboldi A, et al. (2009) C-C chemokine receptor 6-regulated entry of TH-17 cells into the CNS through the choroid plexus is required for the initiation of EAE. *Nat Immunol* 10(5):514–523.
9. Fazekas F, Ropele S, Enzinger C, Seifert T, Strasser-Fuchs S (2002) Quantitative magnetization transfer imaging of pre-lesional white-matter changes in multiple sclerosis. *Mult Scler* 8(6):479–484.
10. Werring DJ, et al. (2000) The pathogenesis of lesions and normal-appearing white matter changes in multiple sclerosis: A serial diffusion MRI study. *Brain* 123(Pt 8):1667–1676.
11. Maggi P, et al. (2014) The formation of inflammatory demyelinated lesions in cerebral white matter. *Ann Neurol* 76(4):594–608.
12. Hofstetter HH, Shive CL, Forsthuber TG (2002) Pertussis toxin modulates the immune response to neuroantigens injected in incomplete Freund's adjuvant: Induction of Th1 cells and experimental autoimmune encephalomyelitis in the presence of high frequencies of Th2 cells. *J Immunol* 169(1):117–125.

13. Brückener KE, el Bayâ A, Galla H-J, Schmidt MA (2003) Permeabilization in a cerebral endothelial barrier model by pertussis toxin involves the PKC effector pathway and is abolished by elevated levels of cAMP. *J Cell Sci* 116(Pt 9):1837–1846.
14. Linthicum DS, Munoz JJBA, Blaskett A (1982) Acute experimental autoimmune encephalomyelitis in mice. I. Adjuvant action of *Bordetella pertussis* is due to vasoactive amine sensitization and increased vascular permeability of the central nervous system. *Cell Immunol* 73(2):299–310.
15. Bettelli E, Baeten D, Jäger A, Sobel RA, Kuchroo VK (2006) Myelin oligodendrocyte glycoprotein-specific T and B cells cooperate to induce a Devic-like disease in mice. *J Clin Invest* 116(9):2393–2402.
16. Herold M, et al. (2015) B7-H1 selectively controls TH17 differentiation and central nervous system autoimmunity via a novel non-PD-1-mediated pathway. *J Immunol* 195(8):3584–3595.
17. Klotz L, et al. (2009) Increased antigen cross-presentation but impaired cross-priming after activation of peroxisome proliferator-activated receptor gamma is mediated by up-regulation of B7H1. *J Immunol* 183(1):129–136.
18. Ortler S, et al. (2008) B7-H1 restricts neuroantigen-specific T cell responses and confines inflammatory CNS damage: Implications for the lesion pathogenesis of multiple sclerosis. *Eur J Immunol* 38(6):1734–1744.
19. Pittet CL, Newcombe J, Antel JP, Arbour N (2011) The majority of infiltrating CD8 T lymphocytes in multiple sclerosis lesions is insensitive to enhanced PD-L1 levels on CNS cells. *Glia* 59(5):841–856.
20. Trabattoni D, et al. (2009) Costimulatory pathways in multiple sclerosis: Distinctive expression of PD-1 and PD-L1 in patients with different patterns of disease. *J Immunol* 183(8):4984–4993.
21. Ben-Nun A, et al. (2014) From classic to spontaneous and humanized models of multiple sclerosis: Impact on understanding pathogenesis and drug development. *J Autoimmun* 54:33–50.
22. Bittner S, et al. (2014) Effects of glatiramer acetate in a spontaneous model of autoimmune neuroinflammation. *Am J Pathol* 184(7):2056–2065.
23. Dai S, Jia R, Zhang X, Fang Q, Huang L (2014) The PD-1/PD-Ls pathway and autoimmune diseases. *Cell Immunol* 290(1):72–79.
24. Kroner A, et al. (2009) Accelerated course of experimental autoimmune encephalomyelitis in PD-1-deficient central nervous system myelin mutants. *Am J Pathol* 174(6): 2290–2299.
25. Sharpe AH, Wherry EJ, Ahmed R, Freeman GJ (2007) The function of programmed cell death 1 and its ligands in regulating autoimmunity and infection. *Nat Immunol* 8(3): 239–245.
26. Talay O, Shen CH, Chen L, Chen J (2009) B7-H1 (PD-L1) on T cells is required for T-cell-mediated conditioning of dendritic cell maturation. *Proc Natl Acad Sci USA* 106(8): 2741–2746.
27. Hirahara K, et al. (2012) Interleukin-27 priming of T cells controls IL-17 production in trans via induction of the ligand PD-L1. *Immunity* 36(6):1017–1030.
28. Greenwald RJ, Freeman GJ, Sharpe AH (2005) The B7 family revisited. *Annu Rev Immunol* 23(1):515–548.
29. Wang S, et al. (2003) Molecular modeling and functional mapping of B7-H1 and B7-DC uncouple costimulatory function from PD-1 interaction. *J Exp Med* 197(9): 1083–1091.
30. Domingues HS, Mues M, Lassmann H, Wekerle H, Krishnamoorthy G (2010) Functional and pathogenic differences of Th1 and Th17 cells in experimental autoimmune encephalomyelitis. *PLoS One* 5(11):e15531.
31. Kebir H, et al. (2007) Human TH17 lymphocytes promote blood-brain barrier disruption and central nervous system inflammation. *Nat Med* 13(10):1173–1175.
32. Huppert J, et al. (2010) Cellular mechanisms of IL-17-induced blood-brain barrier disruption. *FASEB J* 24(4):1023–1034.
33. Manes TD, Pober JS (2014) Polarized granzyme release is required for antigen-driven transendothelial migration of human effector memory CD4 T cells. *J Immunol* 193(12):5809–5815.
34. Kyaw T, et al. (2013) Cytotoxic and proinflammatory CD8+ T lymphocytes promote development of vulnerable atherosclerotic plaques in apoE-deficient mice. *Circulation* 127(9):1028–1039.
35. Choy JC, et al. (2005) Granzyme B induces endothelial cell apoptosis and contributes to the development of transplant vascular disease. *Am J Transplant* 5(3):494–499.
36. Konishi M, et al. (2015) Imaging granzyme B activity assesses immune-mediated myocarditis. *Circ Res* 117(6):502–512.
37. Verneuil L, et al. (2011) Endothelial damage in all types of T-lymphocyte-mediated drug-induced eruptions. *Arch Dermatol* 147(5):579–584.
38. Beecham AH, et al.; International Multiple Sclerosis Genetics Consortium (IMSGC); Wellcome Trust Case Control Consortium 2 (WTCCC2); International IBD Genetics Consortium (IIBDGC) (2013) Analysis of immune-related loci identifies 48 new susceptibility variants for multiple sclerosis. *Nat Genet* 45(11):1353–1360.
39. Hou L, et al. (2015) Type 1 interferon-induced IL-7 maintains CD8+ T-cell responses and homeostasis by suppressing PD-1 expression in viral hepatitis. *Cell Mol Immunol* 12(2):213–221.
40. Ndejembi MP, et al. (2006) Control of memory CD4 T cell recall by the CD28/B7 costimulatory pathway. *J Immunol* 177(11):7698–7706.
41. Kroner A, et al. (2005) A PD-1 polymorphism is associated with disease progression in multiple sclerosis. *Ann Neurol* 58(1):50–57.
42. Huang C-H, et al. (2011) Effects of genetic polymorphisms of programmed cell death 1 and its ligands on the development of ankylosing spondylitis. *Rheumatology (Oxford)* 50(10):1809–1813.
43. Mitchell AL, et al. (2009) Programmed death ligand 1 (PD-L1) gene variants contribute to autoimmune Addison's disease and Graves' disease susceptibility. *J Clin Endocrinol Metab* 94(12):5139–5145.
44. Schwab N, Schneider-Hohendorf T, Wiendl H (2015) Therapeutic uses of anti-α4-integrin (anti-VLA-4) antibodies in multiple sclerosis. *Int Immunol* 27(1):47–53.
45. Latchman YE, et al. (2004) PD-L1-deficient mice show that PD-L1 on T cells, antigen-presenting cells, and host tissues negatively regulates T cells. *Proc Natl Acad Sci USA* 101(29):10691–10696.
46. Litzenburger T, et al. (1998) B lymphocytes producing demyelinating autoantibodies: Development and function in gene-targeted transgenic mice. *J Exp Med* 188(1): 169–180.
47. Bettelli E, et al. (2003) Myelin oligodendrocyte glycoprotein-specific T cell receptor transgenic mice develop spontaneous autoimmune optic neuritis. *J Exp Med* 197(9): 1073–1081.
48. Schneider-Hohendorf T, et al. (2010) Regulatory T cells exhibit enhanced migratory characteristics, a feature impaired in patients with multiple sclerosis. *Eur J Immunol* 40(12):3581–3590.
49. Ruck T, Bittner S, Epping L, Herrmann AM, Meuth SG (2014) Isolation of primary murine brain microvascular endothelial cells. *J Vis Exp* (93):e52204.
50. Weidenfeller C, Schrot S, Zozulya A, Galla H-J (2005) Murine brain capillary endothelial cells exhibit improved barrier properties under the influence of hydrocortisone. *Brain Res* 1053(1-2):162–174.
51. Deli MA, Abrahám CS, Niwa M, Falus A (2003) N,N-diethyl-2-[4-(phenylmethyl)phenoxy] ethanamine increases the permeability of primary mouse cerebral endothelial cell monolayers. *Inflamm Res* 52(Suppl 1):S39–S40.
52. Bittner S, et al. (2013) Endothelial TWIK-related potassium channel-1 (TREK1) regulates immune-cell trafficking into the CNS. *Nat Med* 19(9):1161–1165.
53. De Bock M, et al. (2012) Low extracellular Ca2+ conditions induce an increase in brain endothelial permeability that involves intercellular Ca2+ waves. *Brain Res* 1487: 78–87.